IEEE Access
Multidisciplinary ⋮ Rapid Review ⋮ Open Access Journal

Received 8 June 2023, accepted 21 June 2023, date of publication 26 June 2023, date of current version 30 June 2023.

Digital Object Identifier 10.1109/ACCESS.2023.3289222

RESEARCH ARTICLE

Underwater Image Clarification Based on Double-Opponency Light Estimation and Red Channel Prior

JING QIAN[1,2,3], (Member, IEEE), BIN KONG[1,3,4], (Member, IEEE), AND JING YANG[1,3,5], (Member, IEEE)

[1]Hefei Institutes of Physical Science, Chinese Academy of Sciences, Hefei 230031, China
[2]University of Science and Technology of China, Hefei 230026, China
[3]Peng Cheng Laboratory, Shenzhen 518053, China
[4]Anhui Key Laboratory of Biomimetic Sensing and Advanced Robot Technology, Hefei 230031, China
[5]School of Artificial Intelligence and Big Data, Hefei University, Hefei 230031, China

Corresponding author: Jing Qian (qjjq@mail.ustc.edu.cn)

This work was supported by the Natural Science Foundation of Anhui Province, China, under Grant 2108085MF195.

ABSTRACT Underwater images typically exhibit color bias and low contrast resulting from the absorption and scattering effects of light propagating in water. Such degraded images often have difficulty in satisfying the requirements of underwater operations. Traditional underwater image restoration and enhancement methods generally require long computation times with unsatisfactory results. In this study, we propose a new underwater image restoration method involving background light estimation based on double-opponency and transmission estimation based on the red channel prior. For background light estimation, double-opponency is adopted to imitate human visual color constancy, whereby background light information consistent with human perception is obtained. Transmission estimation uses the prior knowledge that red wavelength has the fastest attenuation in water. To enhance the contrast effect of the resulting image, the restored image is fused with that of contrast stretch processing in HSV space to obtain the final output image. Experiments indicate that the proposed method can reduce computation time by 40% or more relative to comparison methods, thereby producing a clearer normal color image according to both objective and subjective evaluations

INDEX TERMS Underwater image clarification, image processing, computer vision, red channel prior, underwater image.

I. INTRODUCTION

The Earth has abundant marine resources, and using underwater vehicles to perceive the marine environment is an essential means of exploring marine resources. Optical detection is the primary visual perception method of underwater vehicles. In close-range operations, optical images provide higher resolution and richer information with more direct expression than sonar images [1]. Underwater image processing has attracted considerable attention in recent years because of the low cost of image processing implementations. However, underwater light scattering, absorption, and noise, adversely affect the captured underwater images, often resulting in color bias, low contrast, and poor definition [2]. Degraded underwater images can significantly impact the performance of various applications such as underwater archaeology, marine ecological research, underwater surveillance, and underwater target tracking. Therefore, improving the quality of underwater images using image processing technology is crucial for enhancing the performance of underwater applications [3], [4].

Recently, underwater image-clarification technology has made significant advancements in recent times and is now widely utilized, delivering impressive results. Currently, the clarification methods can be broadly divided into two categories: underwater image enhancement and underwater image restoration [5], [6]. The image enhancement method improves contrast and color by adjusting the pixel value of

The associate editor coordinating the review of this manuscript and approving it for publication was Andrea F. Abate.

the image without considering the principle of underwater imaging [7], [8]. The image restoration method is usually based on an underwater imaging physical model that analyzes underwater image degradation mechanisms and estimates image model parameters to clarify the image [9], [10]. However, both image enhancement and image restoration methods require extensive calculations, necessitating long computation times to obtain a clear image [11], [12].

Learning-based underwater image clarification has emerged as a remarkably successful deep learning approach in solving both high- and low-level visual problems [13], [14]. However, learning-based methods need sufficient and effective training data with unique true values. In contrast to the general environment, it is difficult to directly obtain the corresponding clarified ground truth for training networks in an underwater environment, which significantly limits the applicability of the methods. Therefore, learning-based methods are unsuitable for underwater image clarification.

The purpose of our work was to design a less time-consuming underwater image-clarification method with less reliance on training data suitable for real underwater scenes. Our work can provide practical assistance for underwater equipment to detect marine resources quickly. In this study, we mainly focus on the traditional restoration/enhancement methods.

The rest of this paper is organized as follows. In Section II, the relevant work is briefly reviewed. In Section III, after introducing the imaging model, the proposed method is described in detail. In Section IV, the experimental results are presented, including clarified outputs of underwater images from different sources along with objective and subjective evaluations of the resulting images. An analysis and discussion accompany these results. Finally, a summary and future prospects are presented in Section V.

II. RELATED WORK

With the increasing demand for underwater detection equipment, the field of underwater image clarification has drawn considerable attention over the years [15]. Researchers have proposed various methods to address the challenges posed by low contrast, color distortion, blurred texture, and uneven illumination in underwater images. These include underwater image enhancement methods, restoration methods, and hybrid approaches that combine both techniques. These methods can be classified into several types, including color correction, contrast stretching, retinex-based, domain transformation, dehazing-based, optical-model-based, and hybrid methods. In recent years, learning-based methods have been introduced in the field of underwater image clarification, inspired by their success in other domains. In the following section, we present a chronological overview of some of the related methods.

In 2004, Chambah et al. [16] proposed an unsupervised color equalization algorithm inspired by the human visual adaptation mechanism of light and color to facilitate fish segmentation and feature extraction, whereas Schechner and Karpel [17] proposed a method based on the characteristics of backscattered light to improve the visibility of underwater images.

In 2006, Trucco and Olmos-Antillon [18] developed a self-tuning underwater image-restoration algorithm based on a simplified Jaffe-McGlamery model for underwater imaging. The algorithm operated under two ideal assumptions of uniform illumination and scattering only in the forward direction, which are rarely encountered in real-world scenarios. Bazeille et al. [19] presented an automatic pre-processing algorithm that uses several filters, including a homomorphic filter to correct uneven lighting and sharpen the edges, a wavelet filter to suppress noise, and an anisotropic filter to smooth textures and reduce artifacts, thereby performing a histogram-based intensity and color adjustment.

In 2007, Iqbal et al. [20] proposed a sliding stretch algorithm based on a similar distribution hypothesis for histograms of the red (R), green (G), and blue (B) components of an ideal image. The algorithm first stretches the value range of R and G to the range of B in the RGB color space, and then stretches the range of saturation (S) and intensity (I) to [0, 255] in HSI color space.

In 2010, Shi et al. [21] published the ''Underwater image enhancement algorithm based on Contourlet transform and multi-scale Retinex.'' This algorithm first uses a non-subsampled contourlet transform to decompose the underwater image and then applies multi-scale retinex in the low-frequency sub-band to enhance global contrast. However, the algorithm is unsuitable for handling images with insufficient or uneven illumination. Lan et al. [22] proposed a wavelet-based method to reduce backscatter noise in underwater images. After wavelet decomposition, different filters are applied to filter low- and high-frequency coefficients as a trade-off between eliminating noise and preserving details, respectively.

In 2012, based on the well-known dark channel prior (DCP) [23], Chiang and Chen [24] used wavelength compensation and dehazing to reduce the influence of nonuniform auxiliary illumination and improve color fidelity; Ancuti et al. [25] proposed a fusion strategy to enhance underwater images. They first produced a color-corrected and contrast-enhanced version of the original image by using white balancing, temporal bilateral filtering, and local adaptive histogram equalization. Subsequently, they constructed four weight maps consisting of global and local contrast, saliency, and exposure for further multi-scale fusion.

In 2015, Singh et al. [26] presented two recursive algorithms using histogram equalization to enhance images acquired under low-light conditions such as underwater or at night. Both algorithms deal with sub-image histograms in different ways, based on exposure values and predefined thresholds; Singh et al. [27] used wavelet transform to correct the color of underwater images; Li and Guo [28] proposed a hybrid approach that used a simple dehazing algorithm followed by color compensation, histogram equalization, saturation/intensity stretching, and bilateral filtering to obtain

better visibility of underwater images; and Galdran et al. were the first to apply a red channel prior algorithm to underwater images to restore the contrast and color information of the original underwater images [29]. This method is a modification of the classic image defogging model dark channel prior.

In 2017, Zhang et al. [30] extended the multi-scale retinex to CIELAB color space and used a combination of bilateral and trilateral filters on different color channels according to different constraints. While the method effectively mitigates the generation of halo artifacts, its computational complexity is high because of the numerous parameters involved. Vasamsetti et al. [31] presented a framework for a wavelet-based variational enhancement technique for underwater images. By applying wavelet decomposition and a set of energy functionals, they first modified the approximation coefficients of RGB components to adjust the average intensity of the image, and then modified these coefficients at finer scales to correct color and improve contrast; Mhala and Pais [13] presented a CNN based network called underwater image enhancement (UIE)-net for color correction and haze removal to enhance underwater images; Sun et al. [32] proposed another underwater image enhancement model based on encoding–decoding deep CNN networks. The proposed networks were primarily trained and evaluated using certain synthetic datasets. In the literature, the noise environment has been simulated by adding 30, 50, and 70 ml of pure milk to 1 cubic meter of water [32], and underwater images have been synthesized from clean RGB-D images captured on the ground [33].

In 2018, Dai et al. [34] proposed an underwater image enhancement method based on color compensation of bright channels and fusion. Wang et al. [35] presented an algorithm for deblurring and denoising, utilizing a sparse representation of the dark channel image obtained, thereby improving the entropy and average gradient of underwater images.

In 2019, Cai et al. [10] proposed an underwater image restoration method based on scene depth estimation and white balance. However, in cases where the distant view contains numerous texture features, this method may experience misjudgment. Ueda et al. [33] synthesized underwater images based on the modeling of an accurate degradation process considering absorption and scattering as well as ten water types.

In 2020, Li et al. [14] constructed a UIE benchmark (UIEB) and proposed a gated fusion network called Water-Net as a baseline. UIEB includes 950 real-world underwater images, among which 890 have corresponding reference images selected by volunteers from the outputs of 12 existing image enhancement methods. Marques et al. [36] enhanced the contrast, saliency, and color saturation of underwater images by fusing the image information obtained from two different models, and Li et al. [37] designed a balanced color correction algorithm suitable for underwater image enhancement based on prior knowledge of the red channel to improve contrast and brightness.

In 2021, Guo et al. [38] utilized the powerful fitting capabilities of CNN to estimate the illumination image, separating it from the underwater image to obtain the reflectance image, which was considered the final enhanced underwater image; and Hu et al. [39] proposed a novel two-branch deep neural network for underwater image enhancement (UIE), which is capable of separately removing color cast and enhancing image contrast by fully leveraging useful properties of the HSV color space in disentangling chrominance and intensity.

In 2022, Gong and Hu [3] proposed a color compensation method for underwater images by combining Monte Carlo simulation and measured experiments. This method compensates for the color distortion of underwater images and improves the visibility of underwater targets.

In 2023, Kang et al. [40] proposed a perception-aware decomposition and fusion framework for underwater image enhancement (SPDF). This method is built upon the fusion of two complementary pre-processed inputs in a perception-aware and conceptually independent image space. The main advantage of SPDF is that the fusions of different components can be performed separately without any interactions and information loss.

Typically, color correction and contrast stretching techniques can effectively enhance the contrast of an underwater image and partially correct its colors. However, there is a risk of amplifying the noise and introducing artifacts into the image. Domain transformation methods are effective in removing noise from underwater images, but they are limited in addressing other image degradation issues. Dehazing-based methods are time-consuming. Optical model-based methods rely on assumptions and hypotheses that may not hold true in the actual underwater environment. Learning-based methods are highly dependent on training data, and their outputs may not be satisfactory when the real underwater scenario differs significantly from the training data.

In addition to the aforementioned methods, researchers have used techniques from other fields to analyze underwater images. For example, Abunaser et al. [41] utilized particle swarm optimization to reduce the effects of light absorption and scattering in underwater images. New optical imaging devices have been developed to obtain clear images of long-range underwater targets. Although the range and clarity of underwater imaging have improved with the development of laser-scanning underwater imaging and range-gating imaging technology, low cost, low load, and ease of implementation help image-processing technologies maintain their status.

III. METHOD

In the classic optical imaging model, an underwater image I captured by underwater equipment can be regarded as a linear superposition of three influencing factors [42]: the direct component, I_D, which denotes the light reflected by the object, the forward scattering component, I_{FS}, which indicates the deviation of light from its original propagation direction, and the backward scattering component, I_{BS},

which represents the reflection of particles between the object and equipment [8]. The imaging model [43] is expressed as follows:

$$I = I_D + I_{FS} + I_{BS} \tag{1}$$

According to [44], most of the degradation is caused by I_D and I_{BS}, indicating that I_{FS} can be neglected [8]. I_D and I_{BS} can be defined as

$$\begin{cases} I_D = Jt \\ I_{BS} = E(1-t) \end{cases} \tag{2}$$

where J represents the scene radiance of the non-degraded image; E represents the background light; and t denotes transmission. Thus, the underwater image degradation model can be expressed as follows:

$$I_c(x) = J_c(x)t_c(x) + E_c(x)(1 - t_c(x)),\ c \in \{R, G, B\} \tag{3}$$

In Equation (3), $\boldsymbol{x}$ represents the pixel coordinate, and $\boldsymbol{c}$ represents the color channel. I_c represents the acquired input image value of the color channel c; J_C represents the object image to be restored; t_c represents the transmission of the color channel c; and E_c represents the background light of the color channel c [45]. It should be noted that the goal is to recover $J_C(x)$, and thus Equation (3) can be rewritten as follows:

$$J_c(x) = \frac{I_c(x) - E_c(x)}{t_c(x)} + E_c(x),\ c \in \{R, G, B\} \tag{4}$$

In the following section, a new method for clarifying underwater images is proposed. This method first deals with the original underwater image using two independent processes with one process estimating the value of the background light (E_c) and transmission (t_c) to solve major degradation problems and the other process performing contrast stretching. Then, the output of the two processes is subsequently fused in the hue, saturation, value (HSV) color space to obtain the final output image.

A flow diagram of the proposed method is shown in Fig.1, and the details are described in the following subsections.

A. DOUBLE-OPPONENCY BASED COLOR CONSTANCY MODE

Humans have a natural ability to perceive the normal color expressions of objects in the world and can filter out the effects of most color-changing factors to accurately perceive the colors of objects. Visual physiologists have discovered that the double-opponency (DO) color-sensing cells in the primary visual cortex of the human brain are responsible for stable color perception. Gao et al. [46] have demonstrated that the response distribution of DO cells to a color-biased image is highly consistent with the vector that represents the color of the light source in the scene. Based on this finding, they have developed a computational color constancy model that efficiently estimates the color of the light source in the scene. This model uses mostly linear calculations, which has inspired researchers to estimate the light information of underwater images.

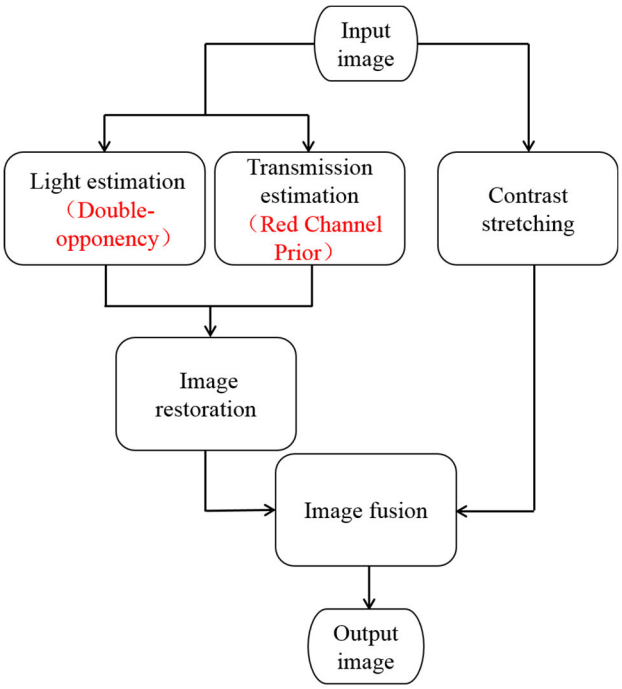

FIGURE 1. Flow diagram of the proposed method.

The perception of color by human vision is a hierarchical process. First, the retina receives input information, which, through the lateral geniculate nucleus (LGN) of the thalamus, reaches the V1 area of the primary and other advanced visual cortices where visual information analysis is processed. Based on the neural mechanism of color processing in the early visual stages, researchers have proposed a computational double-opponency-based color constancy (DOCC) model [42]. In the visual computing model of DOCC, the input image is first transformed from RGB space to LMS space, simulating the long-wavelength (L), medium-wavelength (M), and short-wavelength (S) cone cells responding preferably to red (R), green (G), and blue (B) colors, respectively. Color information is then encoded by color opponency via single-opponent (SO) and double-opponent (DO) cells. DO cells, which are widely present in V1, are capable of detecting the local color contrast between the center and the surroundings of the receptive fields (RF) through spatial transformation, and thus are helpful for color constancy. Finally, the color coding in the visual cortex is transformed into trichromatic space (red, green, and blue) in the higher visual cortex for visual information processing and analysis [47].

B. LIGHT ESTIMATION FROM DOUBLE-OPPONENCY

The primary component of our method is the estimation of underwater light using the DOCC model. A schematic of the process is shown in Fig.2.

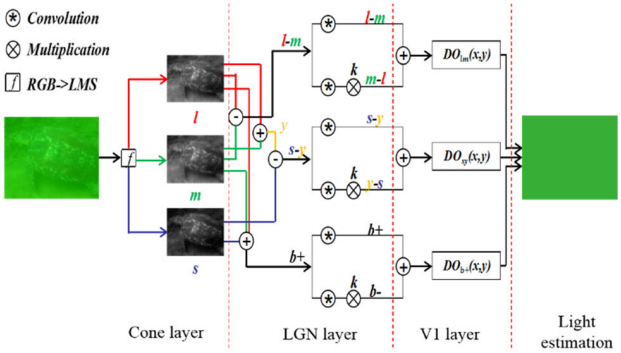

FIGURE 2. Schematic diagram of underwater light estimation (modified based on [46]).

1) LMS SPATIAL EXPRESSION OF CONE CELLS

Corresponding to the first stage of visual perception, in which the L, M, and S cones of the retina encode the information entering the eye, the image from the RGB space is converted to the LMS spatial expression of cone cells, with the help of XYZ color space.

According to the standard issued by the International Telecommunication Union, the relationship between the RGB and LMS color spaces can be expressed as follows [47]:

$$\begin{bmatrix} L \\ M \\ S \end{bmatrix} = \begin{bmatrix} 0.3192 & 0.6089 & 0.0447 \\ 0.1647 & 0.7638 & 0.0870 \\ 0.0202 & 0.1295 & 0.9391 \end{bmatrix} \begin{bmatrix} R \\ G \\ B \end{bmatrix} \tag{5}$$

2) SINGLE-OPPONENCY RESPONSE IN LGN LAYER

According to Equation (6), the spatial information of LMS is transformed into single opponency (denoted as O):

$$\begin{cases} \begin{bmatrix} O_{lm} \\ O_{ys} \\ O_{b+} \end{bmatrix} = Tran. * \begin{bmatrix} L \\ M \\ S \end{bmatrix}, \begin{bmatrix} O_{ml} \\ O_{sy} \\ O_{b-} \end{bmatrix} = - \begin{bmatrix} O_{lm} \\ O_{ys} \\ O_{b+} \end{bmatrix} \\ Tran. = \begin{bmatrix} \frac{1}{\sqrt{2}} & \frac{-1}{\sqrt{2}} & 0 \\ \frac{1}{\sqrt{6}} & \frac{1}{\sqrt{6}} & \frac{-2}{\sqrt{6}} \\ \frac{1}{\sqrt{3}} & \frac{1}{\sqrt{3}} & \frac{1}{\sqrt{3}} \end{bmatrix} \end{cases} \tag{6}$$

In Equation (6), the subscripts l, m, and s represent the three components of the input image in LMS space; y is the synthetic yellow component given by $y = m + s$, and b is the luminance component given by $b = l + m + s$. *Tran.* denotes the transformation ratio.

The response of the receptive fields (denoted as SO) is then calculated using Gaussian convolution. Equation (7) provides an example of blue excitation/yellow inhibition opponency:

$$SO_{s+y-}(x, y; \sigma) = O_{sy}(x, y) \otimes RF(x, y; \sigma) \tag{7}$$

In formula (7), "+" is used for excitation and "-" for inhibition; $\otimes$ denotes convolution; σ specifies the size of the receptive field, and RF describes the structure of the receptive field.

3) DOUBLE-OPPONENCY IN V1 LAYER

In the V1 cortex, two single opponents with different receptive field sizes work together to form a double-opponency response (DO), given by formula (8):

$$\begin{cases} DO_{lm}(x, y) = SO_{l+m-}(x, y; \sigma) + k \cdot SO_{m+l-}(x, y; \lambda\sigma) \\ DO_{sy}(x, y) = SO_{s+y-}(x, y; \sigma) + k \cdot SO_{y+s-}(x, y; \lambda\sigma) \\ DO_{b+}(x, y) = SO_{b+}(x, y; \sigma) + k \cdot SO_{b-}(x, y; \lambda\sigma) \end{cases} \tag{8}$$

In formula (8), σ defines the size of center receptive field, and $\lambda\sigma$ defines the size of the surrounding receptive field which in general, is three times that of the central receptive field, *i.e.* $\lambda = 3$. The parameter $k \in [0, 1)$ denotes the weight of the surrounding receptive field. When $k = 0$, the effect of surrounding receptive field is ignored.

4) COLOR SENSING IN HIGHER VISUAL CORTEX

Finally, in the high-level visual cortex, the signals are transferred back to LMS space to obtain color information according to Equation (9).

$$\begin{bmatrix} DT_l \\ DT_m \\ DT_s \end{bmatrix} = Tran.^{-1} * \begin{bmatrix} DO_{lm} \\ DO_{sy} \\ DO_{b+} \end{bmatrix} \tag{9}$$

Similar to various existing models, we assumed that the scene is illuminated by a single light source with a spatially uniform color across the scene [46]. Finally, the color of the background light, E_{lms}=(E_l, E_m, E_s), is estimated as follows:

$$\begin{cases} E_i = \max(DT_i) / \sum f \\ \sum f = \sum_{i \in \{l,m,s\}} \max(DT_i) \end{cases} \quad i \in \{l, m, s\} \tag{10}$$

For display and subsequent use, it is necessary to transfer the E_{lms} in LMS space to E_{rgb} in RGB space. The transformation is given by Equation (11).

$$E_{rgb} = \begin{bmatrix} E_R \\ E_G \\ E_B \end{bmatrix} = \begin{bmatrix} 5.3341 & -4.2829 & 0.1428 \\ -1.1556 & 2.2581 & -0.1542 \\ 0.0448 & -0.2195 & 1.0831 \end{bmatrix} \begin{bmatrix} E_l \\ E_m \\ E_s \end{bmatrix} \tag{11}$$

Fig.3 shows the results of underwater light estimation.

Based on subjective vision, the estimated light information in Fig.3 is consistent with human visual results.

C. TRANSMISSION ESTIMATION BASED ON RED CHANNEL PRIOR

In contrast to the attenuation of the wavelength in air, the colors associated with different wavelengths have different attenuation rates in water, with the red wavelength intensity decaying faster as distance increases. To account for this specific characteristic of underwater environments, researchers have modified the dark channel prior [23] and proposed a red channel prior:

$$\min(\min_{y \in \Omega(x)} (1 - J_R(y)), \min_{y \in \Omega(x)} (J_G(y)), \min_{y \in \Omega(x)} (J_B(y))) \approx 0 \tag{12}$$

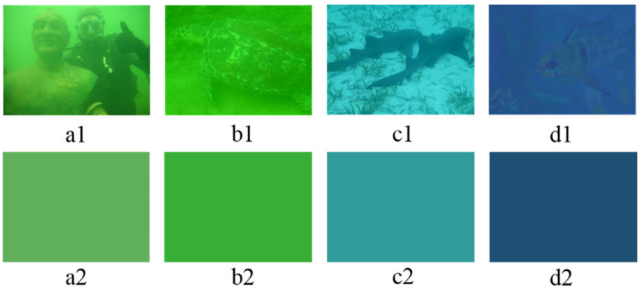

FIGURE 3. Light source estimation result. The first row is the original image; the second row is the corresponding light estimation such that light estimate for a1 is a2.

In Equation (12), $\Omega(x)$ is the neighborhood of pixels around location x. In the literature, Galdran et al. [29] deduced the transmission in detail based on red-channel prior, whereby the transmission of $t_c(x)$ is estimated by Equation (13):

$$\begin{cases} t_R(x) = 1 - \min(\frac{\min\limits_{y\in\Omega(x)}(1-I_R(y))}{1-E_R}, \frac{\min\limits_{y\in\Omega(x)} I_G(y)}{E_G}, \frac{\min\limits_{y\in\Omega(x)} I_B(y)}{E_B}) \\ t_G(x) = t_R(x)^{\lambda_G} \\ \\ t_B(x) = t_R(x)^{\lambda_B} \end{cases} \tag{13}$$

In Equation (13), λ_G and λ_B are attenuation coefficients, which depend on the type of water. However, determining the type of water can be challenging, and thus it can be difficult to accurately determine the values of λ_G and λ_B. From experiments and using Equation (3), Galdran et al. simplified the image restoration formula by directly constructing the transmission t(x). $t(x)$ is the transmittance estimated considering saturation. Artificial light sources are common in underwater images, and the illumination area of the artificial light sources may affect the perception of transmittance. Therefore, it is necessary to consider saturation in the calculation of transmittance. Finally, the saturation of $Sat(I)$ and transmission of $t(x)$ are defined as follows:

$$\begin{cases} t(x) = 1 - \min\left\{ \frac{\min\limits_{y\in\Omega(x)}(1-I_R(y))}{1-E_R}, \frac{\min\limits_{y\in\Omega(x)} I_G(y)}{E_G}, \frac{\min\limits_{y\in\Omega(x)} I_B(y)}{E_B}, \right. \\ \qquad \left. \lambda \min\limits_{y\in\Omega(x)} Sat(y) \right\} \\ \\ Sat(I) = \frac{\max(I_R,I_G,I_B)-\min(I_R,I_G,I_B)}{\max(I_R,I_G,I_B)} \end{cases} \tag{14}$$

In Equation (14), $\lambda \in [0, 1]$ is a scalar multiplier that can be manually adjusted as required. In this study, $\lambda = 0.23$. Fig. 4 shows the results for $t(x)$ and 1- $t(x)$.

D. FINAL IMAGE RESTORATION

Based on the E_{rgb} estimation of background light and transmittance $t(x)$ calculated directly, a simplified formula for image restoration is given as follows:

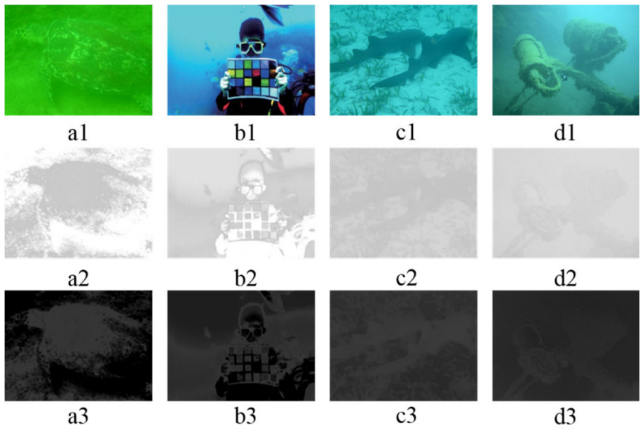

FIGURE 4. Estimated transmittance $t(x)$ and 1 - $t(x)$.

$$\begin{cases} J_R(x) = \frac{I_R(x)-E_R(x)}{\max(t(x),t_0)} + (1-E_R(x))E_R(x) \\ J_G(x) = \frac{I_G(x)-E_G(x)}{\max(t(x),t_0)} + (1-E_G(x))E_G(x) \\ J_B(x) = \frac{I_B(x)-E_B(x)}{\max(t(x),t_0)} + (1-E_B(x))E_B(x) \end{cases} \tag{15}$$

In formula (15), t_0 is a small value that prevents the denominator from being too small; a typical value of t_0 is 0.1.

Fig.5 shows the results of the restored image.

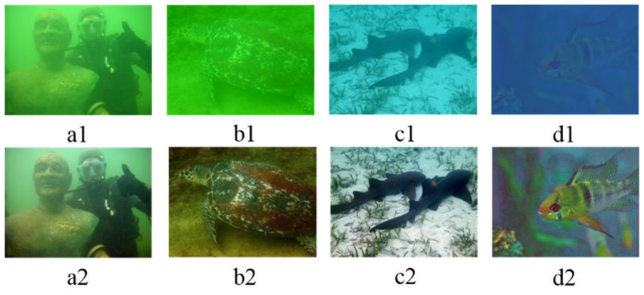

FIGURE 5. Results of image restoration.

It can be seen from Fig.5 that the restoration method has a good corrective effect on the color-bias of the original image.

E. CONTRAST STRETCHING

Several underwater images display low contrast because of the scattering effect of suspended particles in water. A simple way to deal with this problem is to stretch the contrast by changing the distribution of pixel values. Various algorithms for contrast stretching are available, and the choice of algorithm depends on the specific requirements of the user. For example, we use the following algorithm:

First, histograms of the R, G, and B values of the original image are calculated. Then, the values close to 0 or 255 are cut out according to a proportion (2% for instance) of the total pixels whereby the minimum value (denoted as V_{min}) and maximum value (denoted as V_{max}) of the residual pixels

are deter1mined. Finally, the pixel values from $[V_{min}, V_{max}]$ are mapped to [0, 255] using Equation (16).

$$F(\Omega)_{\Omega\in(R,G,B)} = \begin{cases} 0 & f(\Omega) \le V_{\min}(\Omega) \\ 255 & f(\Omega) \ge V_{\max}(\Omega) \\ \frac{f(\Omega)-V_{\min}(\Omega)}{V_{\max}(\Omega)-V_{\min}(\Omega)} * 255 & other \end{cases} \tag{16}$$

where $F(\Omega)$ is the value of each pixel in the R, G, or B channels; $V_{\min}(\Omega)$ and $V_{\max}(\Omega)$ represent the minimum and maximum pixel values selected in each channel, respectively. The effects of contrast stretching are illustrated in Fig. 6.

In Fig. 6, the application of the contrast-stretching technique results in a significant improvement in the brightness and contrast of the images, as well as an enrichment of color information. However, an adverse edge effect is observed.

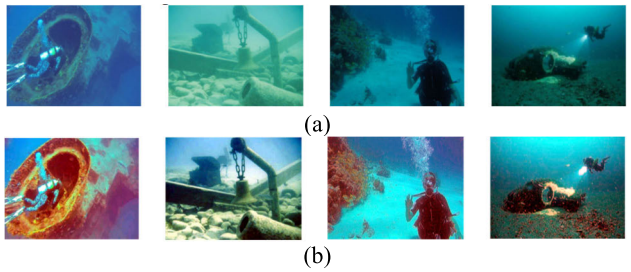

FIGURE 6. Results of contrast stretching process: (a) original images; (b) stretched images.

F. IMAGE FUSION

In the previous steps, a restoration image (RI) and contrast stretch image denoted as LS were obtained. The restored image primarily considers the light absorption of water, which affects the pixel color. The contrast stretch image mainly focuses on the light-scattering effect of water, and this affects pixel intensity. The improved parts of the two images are fused to enhance the visual effect. Thus, the HSV color space is very suitable for such a fusion process. The fusion strategy is shown in Fig. 7.

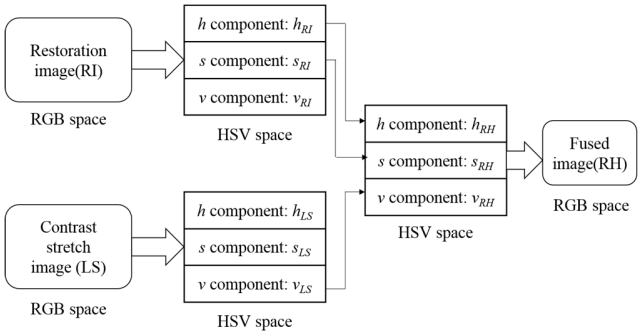

FIGURE 7. Image fusion process.

The execution of the image fusion process is outlined in the following steps:

1) Transform the color restoration image RI and contrast stretch image LS from RGB to HSV space.

2) Consider the hue component h_{RI} and saturation component s_{RI} of the color restoration image RI as the hue component h_{RH} and saturation component s_{RH} of the fused image RH, respectively. The value component v_{LS} of the contrast stretch image LS, is the value component v_{RH} of the fused image RH, that is:

$$h_{RH} = h_{BC},\ s_{RH} = s_{BC},\ v_{RH} = v_{LS} \tag{17}$$

3) Transform the fused image RH from HSV to RGB space to obtain the final output image.

Fig. 8 shows sample images illustrating the results of the proposed method.

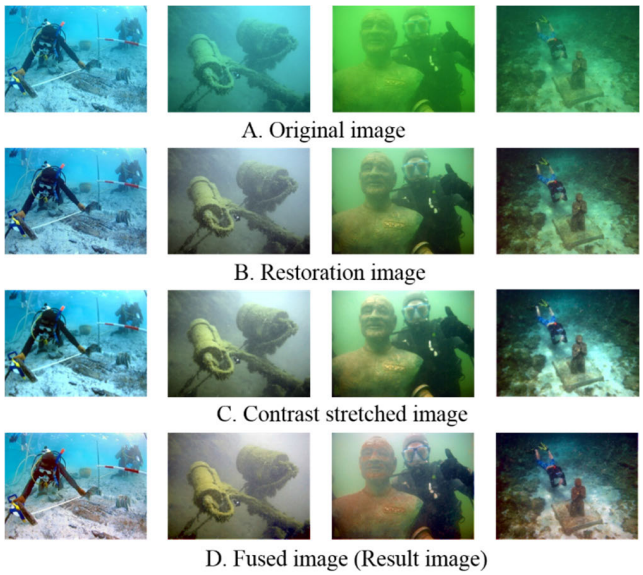

FIGURE 8. Result images of the proposed method.

In Fig.8, the resulting image provides better subjective visual perception than the original image.

IV. EXPERIMENT AND ANALYSIS

In this section, the experimental results presented utilized two different sources of data. We created a dataset of 310 underwater images, which we refer to as Underwater Images by Searching the Internet (UISI), by searching the internet for one of the sources and collecting images with varying qualities from webpages with diverse content and purposes. The other source consisted of three open datasets: real-world underwater image enhancement (RUIE) [48], third underwater robot picking (URPC2019) [49] and Underwater Image Enhancement Benchmark (UIEB) [14] datasets. All comparative data were obtained using the same equipment.

In the following section, sample images are provided to demonstrate the visual effects of the proposed method along with objective and subjective evaluations of the resulting images with accompanying analysis and discussion. To evaluate the effectiveness of our proposed underwater

double-opponency red-channel-prior (UDR) image clarification, we selected four different methods of various types from recent literature and implemented them on a computer for comparison. The first method is based on dark channel prior (DCP) [10], which is a classic underwater image restoration method. The second method is based on color compensation (CC) [3], which is a classic underwater image enhancement method. The third method is based on information fusion (IF) [36], a state-of-the-art method published at the CVPR conference in 2020. Note that IF is particularly useful for repairing degraded images with insufficient underwater illumination, as shown in the fourth sample in Fig. 11. The other two methods, namely automatic red-channel underwater image restoration (ARR) [29] and simple estimation of red channel's transmittance for underwater image enhancement (SRE) [37], also utilize red channel prior.

A. EXPERIMENT ON UISI DATASET

The UISI image set contains 310 underwater images of different qualities. All images were collected from webpages with various contents and purposes, and a portion of them were extracted from videos captured underwater. The original sizes and aspect ratios of these images differ, and all images were resized to 640×480 pixels. To facilitate analysis of the effect of clarification results, we organized these 310 images and assigned each image an index number as follows:

- There were 182 images from webpage illustrations. These images were divided into four groups according to their degree of clarity, from high to low, based on personal observation. Group-1 had 32 images with the highest image quality, and indices 1 to 32 were assigned to these images. Group-2 contained 83 images, with indices ranging from 33 to 115. Group-3 contained 54 images, with indices ranging from 116 to 169. Group-4 contained 13 images, with indices ranging from 170 to 182.
- There were 114 images from snapshots of three different videos on webpages. These images were assigned indices of 183 to 296, with indices of 183 to 235 for the first video, 236 to 285 for the second video, and 286 to 296 for the third video. These images are referred to as group-5 in this paper.
- There were 14 randomly selected images from the URPC2019 dataset. Their indices ranged from 297 to 310, and are referred to as group-6 in this paper.

Fig. 9 shows six samples from the UISI, from each of the groups described above.

Fig.10 shows the difference in underwater image contrast measure (UIConM) before and after fusion. UIConM is a contrast evaluation index for underwater images, as proposed by Panetta et al. [50]. Higher UIConM values indicate better contrast.

In Fig.10, the abscissa value denotes the index number of an image in the UISI dataset and the ordinate value is the difference between the UIConM value of the fused and restored images. Note that after fusing the restored image with the contrast-stretched image, the low-contrast restored image is improved, and in general, the contrast of the fused image is higher than that of the restored image.

FIGURE 9. Sample images in UISI dataset.

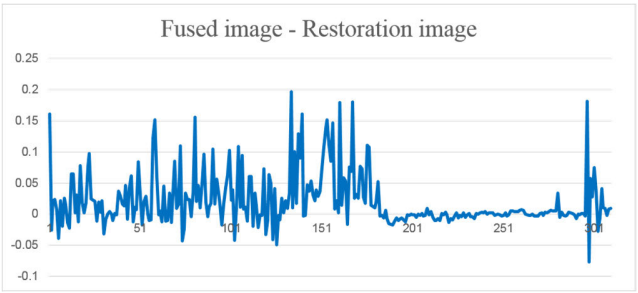

FIGURE 10. UIConM difference between fused and restored images.

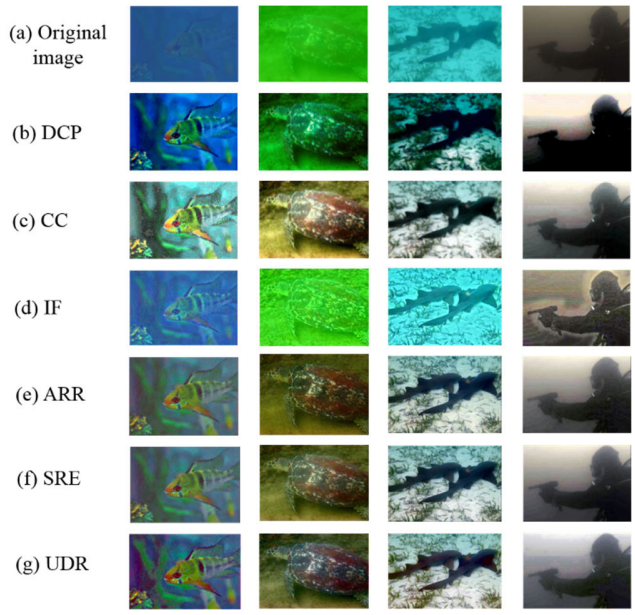

FIGURE 11. Examples of clarification results by different methods: (a) original and result images by (b) DCP, (c) CC, (d) IF, (e) ARR, (f) SRE and (g) UDR (our method).

Fig.11 shows examples of UISI images clarified using different methods. The first row represents the original image. The second, third, fourth, fifth, and sixth lines show the image clarification results of using DCP, CC, IF, ARR, and SRE,

respectively. The last line shows the images resulting from the proposed method.

From a human perspective based on visual observations of Fig.11, the proposed method eliminates the blurring effect caused by light scattering to a certain extent, producing clearer images. This process has a positive effect on color recovery, making the resulting images more consistent with the color perception of the human eye in natural environments.

B. PERFORMANCE EVALUATION

The performance of the proposed method was evaluated by applying objective and subjective quality criteria to the resulting images. The objective evaluation was conducted by computing quality indicators, and the subjective evaluation was based on observations and scoring [51]. The program execution times were also recorded.

Researchers have proposed several indicators for evaluating image quality. The suitability of the indicators differs depending on the purpose and applications. Owing to the absence of ground truth references in real underwater environments, we opted to use commonly used no-reference image quality assessment measures instead of the peak signal-to-noise ratio (PSNR) full-reference measure commonly used in natural environments. We selected measures such as the underwater image quality measure (UIQM), underwater image contrast measure UIconM [50], and underwater color image quality evaluation (UCIQE) [52] to better suit the characteristics of underwater images and the purpose of image clarification

1) TIME COST

In many practical applications, the time required for image processing is very critical. Experiments were conducted on UISI to compare the processing times of the different methods applied to each image, thereby to find out that UDR was the fastest; CC was the second fastest; DCP, SRE, and ARR were similar in terms of time cost, and IF was the slowest. In Fig. 12 a plot of the processing times is displayed. Upon calculating the ratio of the computation time of UDR to that of CC, a maximum value of 40.38% and minimum value of 32.15% were obtained. Group averages of the processing times and the UDR/CC ratio are listed in Table 1.

From the data, we know that the proposed UDR method can reduce the time cost of the image-clarification process to less than half of that of the comparison methods.

2) UIQM AND UICONM

Inspired by the human visual system, Panetta et al. [50] proposed a no-reference underwater image quality assessment method, UIQM. This method considers the degradation mechanism and imaging characteristics of underwater images, using underwater image colorfulness measure (UICM), underwater image sharpness measure (UISM), and

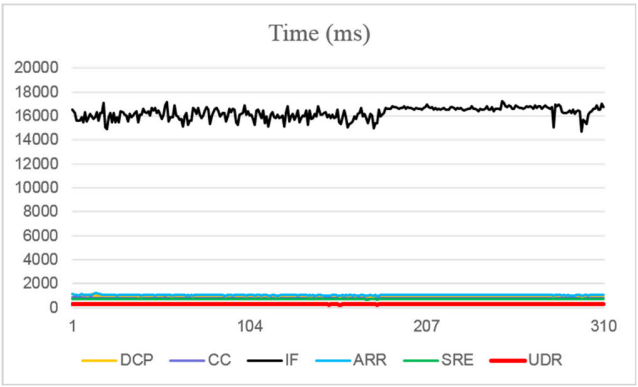

FIGURE 12. Comparison of the processing times of different methods applied to each image in UISI.

TABLE 1. Group averages of the processing times using different methods (unit: ms).

Group	DCP	CC	IF	ARR	SRE	UDR	UDR/CC
1	971.6	801.0	15923.9	1084.7	718.6	279.8	34.93%
2	933.0	775.1	16131.3	1055.5	710.4	273.7	35.31%
3	925.9	768.2	15978.3	1036.8	705.5	270.1	35.16%
4	921.6	753.7	15877.3	1021.2	698.4	266.5	35.36%
5	927.4	787.7	16637.9	1051.9	708.4	271.7	34.50%
6	931.7	781.1	16220.9	1051.9	713.1	280.8	35.95%
Avg.	933.1	780.6	16262.9	1052.4	709.3	273.0	34.97%

UIConM as the basis for assessing the quality of underwater images. The value of *UIQM* can be obtained as follows:

$$UIQM = \beta_1{}^{*}UICM + \beta_2{}^{*}UISM + \beta_3{}^{*}UIConM \quad (18)$$

In Equation (18), β_1, β_2, and β_3 are weight factors that are typically set to $\beta_1 = 0.0282$, $\beta_2 = 0.2953$, and $\beta_3 = 3.5753$. Moreover, because contrast is considered a better evaluation indicator for image restoration problems, UIConM is usually chosen to measure the contrast quality of an image. With both UIQM and UIConM, the higher the value, the better it is.

Figs.13 and 14 show the improvements in UIQM and UIconM after using the proposed method for the processing of the images in the UISI dataset. The abscissa represents the index number of the image in the UISI dataset. The ordinate value represents the difference between the processed and original images.

Figs.15 and 16 display the group averages of UIQM and UIconM, respectively for each group in the UISI dataset after different clarification processes.

In addition, in Figs.13 to 16 following the clarification process, most images in UISI have improved UIQM and UIconM; however, for some of the video snapshots (in group-5 with index 183 to 296), the improvement is not obvious, and the values appear almost the same for all indices. This is because these three underwater videos are for people to enjoy, and the picture quality is relatively good and approximately the same for the entire video.

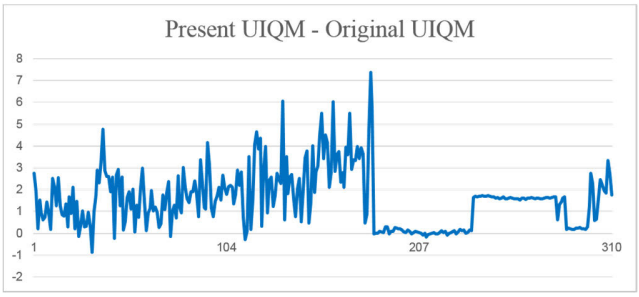

FIGURE 13. Improvement in UIQM by the proposed method.

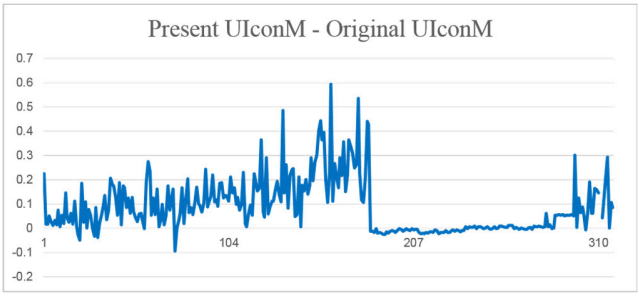

FIGURE 14. Improvement in UIconM by the proposed method.

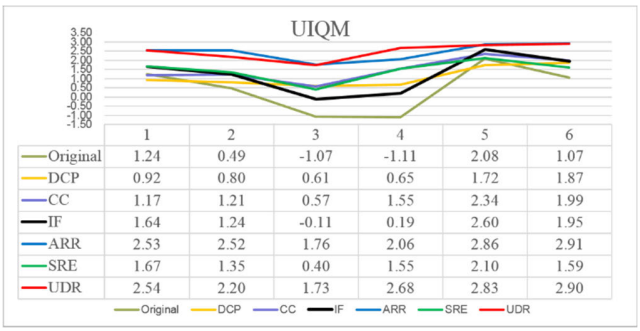

	1	2	3	4	5	6
Original	1.24	0.49	-1.07	-1.11	2.08	1.07
DCP	0.92	0.80	0.61	0.65	1.72	1.87
CC	1.17	1.21	0.57	1.55	2.34	1.99
IF	1.64	1.24	-0.11	0.19	2.60	1.95
ARR	2.53	2.52	1.76	2.06	2.86	2.91
SRE	1.67	1.35	0.40	1.55	2.10	1.59
UDR	2.54	2.20	1.73	2.68	2.83	2.90

FIGURE 15. Group averages of UIQM for each clarification process.

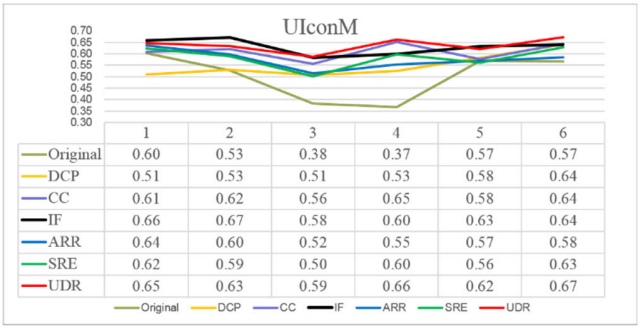

	1	2	3	4	5	6
Original	0.60	0.53	0.38	0.37	0.57	0.57
DCP	0.51	0.53	0.51	0.53	0.58	0.64
CC	0.61	0.62	0.56	0.65	0.58	0.64
IF	0.66	0.67	0.58	0.60	0.63	0.64
ARR	0.64	0.60	0.52	0.55	0.57	0.58
SRE	0.62	0.59	0.50	0.60	0.56	0.63
UDR	0.65	0.63	0.59	0.66	0.62	0.67

FIGURE 16. Group averages of UIconM for each clarification process.

3) UNDERWATER COLOR IMAGE QUALITY EVALUATION UCIQE

Yang and Sowmya [52] used chromaticity, saturation, and contrast as measuring components and combined them linearly to obtain a quality evaluation method, called UCIQE, which can quantify non-uniform color deviation, blur, and contrast of underwater images. First, the underwater image is transformed from RGB to CIELab color space, which is more consistent with human visual perception. The measurement components representing the underwater image quality are calculated, whereby UCIQE is expressed as follows:

$$UCIQE = \omega_1{}^*\sigma + \omega_2{}^*con + \omega_3{}^*\mu \tag{19}$$

In Equation (19), σ is the standard variance of chroma; con denotes brightness contrast; μ is average saturation; and ω_1, ω_2, and ω_3 are the weight factors of linear combinations. Typically, the weight factors are selected as $\omega_1 = 0.4680$, $\omega_2 = 0.2745$, and $\omega_3 = 0.2576$. The higher UCIQE values indicate better image contrast.

Fig. 17 shows the improvement in UCIQE after using the proposed method to process the images in the UISI dataset. The abscissa represents the index number of the image in the UISI dataset. The ordinate value represents the difference between the processed and original images.

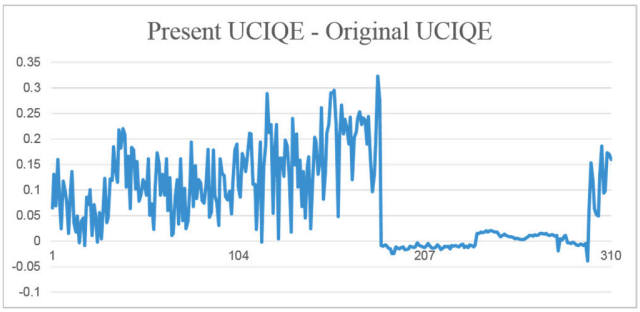

FIGURE 17. Improvement in UCIQE after using the proposed method.

In Figs. 17 and 18, most images in the UISI dataset have improved UIQCE after the clarification process. The proposed method has the highest UCIQE value for most groups among the comparison methods.

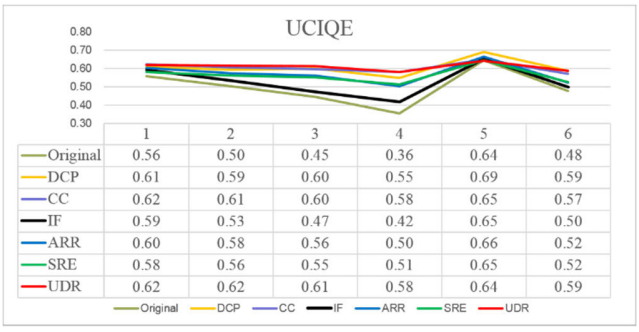

	1	2	3	4	5	6
Original	0.56	0.50	0.45	0.36	0.64	0.48
DCP	0.61	0.59	0.60	0.55	0.69	0.59
CC	0.62	0.61	0.60	0.58	0.65	0.57
IF	0.59	0.53	0.47	0.42	0.65	0.50
ARR	0.60	0.58	0.56	0.50	0.66	0.52
SRE	0.58	0.56	0.55	0.51	0.65	0.52
UDR	0.62	0.62	0.61	0.58	0.64	0.59

FIGURE 18. UCIQE for the clarification processes applied to each group in the UISI image set.

According to the objective statistical assessment results, the proposed method displays a better processing effect on the original image.

4) SUBJECTIVE EVALUATION

Automation of underwater operating equipment is an inevitable development trend. However, limited by current

technology, a large number of underwater tasks still require manual teleoperation. Therefore, understanding the subjective observational effect of the human eye on underwater images is crucial. We conducted a subjective evaluation and obtained encouraging results.

a: DESIGN OF THE EVALUATION METHOD

Subjective evaluation of the quality of an image involves viewing the image with the human eye and then providing a quantitative grade score. Here, in designing the scoring scheme, the concern is the improvement in visual effect provided by different image-clarification methods. Therefore, the following scoring scheme was designed.

Selected individuals observed a pair of images before and after the clarification process simultaneously, compared the images, and then scored and recorded the degree of improvement in visual image quality according to personal judgment. A 10-point scoring system was used, where 0 denotes no obvious difference that can be perceived from an image pair, and 1 to 10 denote different degrees of improvement with higher scores indicating greater degree of improvement. Considering that in certain cases, the image quality may deteriorate after the clarification process, we also defined negative scores, -1 to -5, to indicate different degrees of image quality degradation (the higher the negative score, the worse was the quality).

b: SUBJECTIVE EVALUATION EXPERIMENT

For the convenience of comparison and scoring, the images were prepared for evaluation as follows: The original underwater image was combined with the six clarified images obtained using different methods (i.e., DCP, CC, IF, ARR, SRE, and UDR) into one picture and presented to the evaluators. The images to be evaluated included all individual images in group-1 to group-4 and group-6 in addition to four images from group-5. Because the picture quality of the video was relatively good and the same across the entire video, four images from group-5 were randomly selected. So, there were a total of 200*6 pairs of images to evaluate.

Teachers and students from four different research institutions and universities were invited with 25 volunteers participating in the experiment. All evaluators used their free will to score according to the above definition. Among the volunteers, the gender distribution was:18 males and 7 females, whereas the age distribution was:13 persons between 18 to 23 years old, 8 persons between 24 to 29 years old, and 4 persons above 29 years old.

Subsequently, statistical analyses were performed on the above scoring results.

c: EVALUATION RESULTS

Generally, there are significant differences in people's subjective consciousness, such as in the visual evaluation of image quality. The variable values in the score data reflect our original intention in designing the subjective evaluation method, that is, to provide the evaluator sufficient freedom to exert subjective volition. However, still some regular trends were observed.

By comparing the score data, we found that, although there were significant differences in the score values of different evaluators for the same image pair, the comparison of the high or low levels among different image pairs by each evaluator revealed statistical consistency overall. That is, of the 25 evaluators, some gave relatively high scores to all pairs, whereas others gave relatively low scores to all pairs. Therefore, we took the average of the 25 scores of a pair as the subjective evaluation score.

Fig.19 shows a plot of the subjective scores of 200 × 6 pairs obtained by the six methods: DCP, CC, IF, ARR, SRE, and UDR. The abscissa value is the re-indexed number of 200 images, which ignores the index numbers of most video snapshots and makes the remaining numbers continuous. The ordinate value is the subjective evaluation score.

Group averages of subjective evaluation scores are presented in Fig. 20.

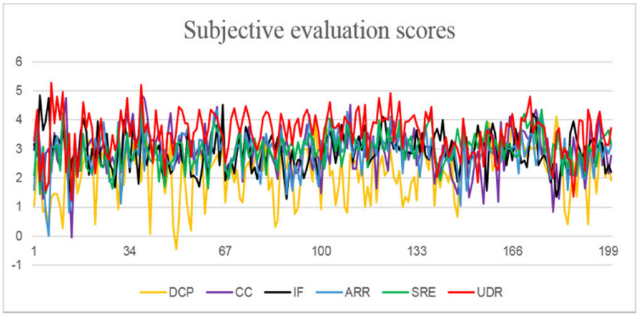

FIGURE 19. Subjective evaluation scores after DCP, CC, IF, ARR, SRE, and UDR processing.

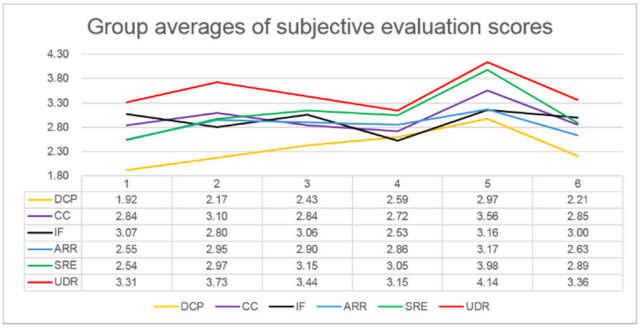

FIGURE 20. Comparison of group averages of subjective evaluation scores on images processed by different methods.

In Figs.19 and 20, we observe that the perceived image quality of most images in UISI is improved to varying degrees by all six methods. Compared with the other methods, the proposed method provides the best subjective visual enhancement effect in most images; CC, IF, ARR, and SRE are similar in group average scores, and DC has the lowest score in most groups.

The subjective evaluation results also show that the proposed image-clarifying SDR method is promising.

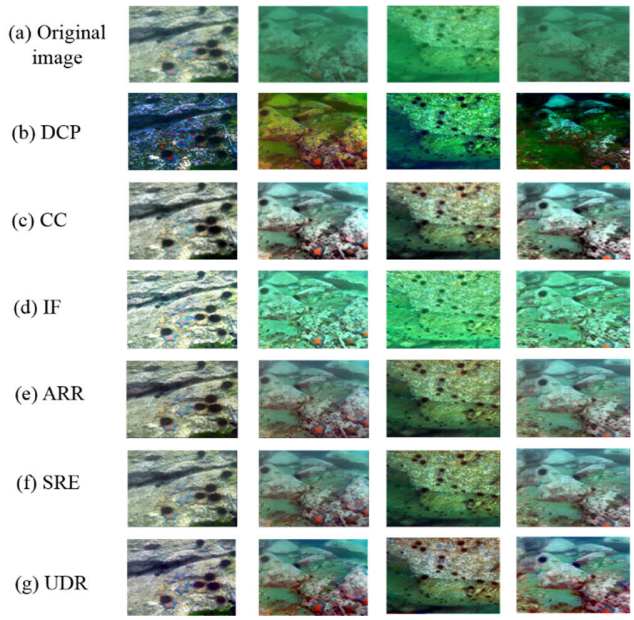

FIGURE 21. Applying six clarification methods to RUIE data: (a) original images, and the resulting images after processing by (b) DCP, (c) CC, (d) IF, (e) ARR, (f) SRE, and (g) proposed UDR.

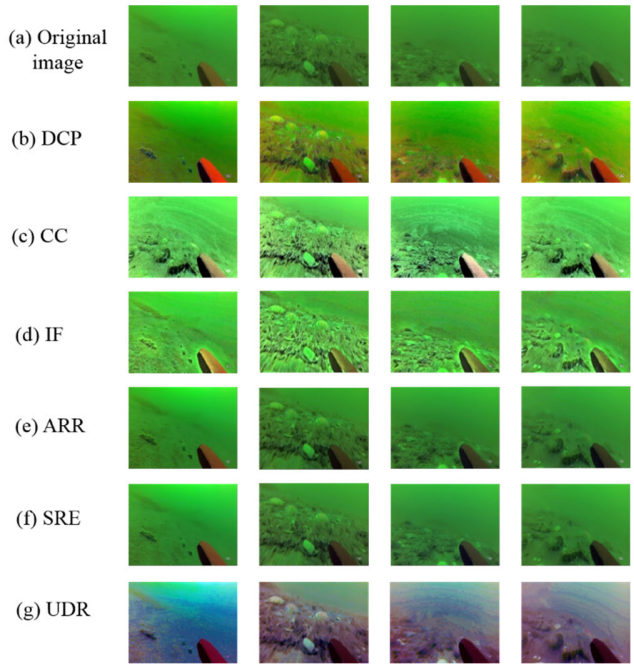

FIGURE 22. Applying six clarification methods to URPC2019 data: (a) original images, and the resulting images after processing by (b) DCP, (c) CC, (d) IF, (e) ARR, (f) SRE, and (g) proposed UDR.

V. EXPERIMENT ON RUIE AND URPC2019 DATA

To verify the effectiveness of the proposed method, underwater images from RUIE, URPC2019 and UIEB datasets were processed. The results are presented in Figs. 21, 22 and 23.

Figs. 21, 22 and 23 show that the proposed UDR method can improve the quality of the original image as well as the color and texture of the sea urchins in Figs. 21 and 22; sea cucumbers are also clearer in the resulting image. However, when camera movement causes blurring in the original image, the wrong image color appears. In addition, the proposed method will introduce pseudo-textures when there are large uniform regions in the image.

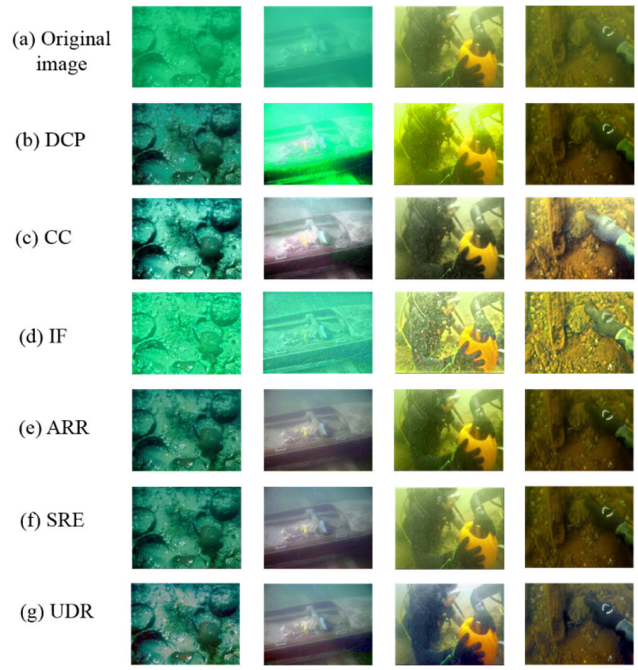

FIGURE 23. Applying six clarification methods to UIEB data: (a) original images, and the resulting images after processing by (b) DCP, (c) CC, (d) IF, (e) ARR, (f) SRE, and (g) proposed UDR.

VI. SUMMARY

To address the problems of color bias and low contrast in underwater images, we proposed an underwater image restoration method based on human visual color constancy using double opponency and red channel prior. First, the original image is converted from RGB space to LMS space; the signals are linearly combined; and Gaussian convolutions are performed to imitate the function of receptive fields. Second, two receptive fields of different sizes work jointly to elicit a double-opponency response. Subsequently, estimated underwater light values are combined with the red channel prior model of the underwater image, to obtain a color-compensation image for correct perception of color information. Simultaneously, to reduce the color distortion caused by water scattering, traditional contrast stretching is performed on the original image, to obtain the contrast-stretch image. Finally, the improved parts of the two images are fused to enhance the visual effect.

In this study, using prior knowledge of human visual perception and the attenuation law of different wavelengths in water, the proposed method corrects the color of underwater images for accurate color perception. Combined with traditional image enhancement and fusion methods, this method can realize underwater image restoration in less computa-

tion time. Compared with other traditional image restoration or enhancement methods, the proposed method for image clarification provides a greater advantage in terms of computation time while ensuring image quality both objectively and subjectively.

Further work is still required, in particular, to improve the restoration effect of images with insufficient underwater illumination, time cost optimization, and elimination of pseudo-texture phenomena.

CREDIT AUTHORSHIP CONTRIBUTION STATEMENT

Jing Qian: Conceptualization, software, methodoloy, writing-original draft, and data curation. Bin Kong: Writing-review and editing, and supervision. Jing Yang: Project administration, writing-review, supervision, and validation.

DECLARATION OF COMPETING INTEREST

The authors declare that they have no know competing financial interests or personal relationships that could have appeared to influence the work reported in this article.

ACKNOWLEDGMENT

The authors would like to thank Prof. Xianping Fu from the Information Science and Technology College, Dalian Maritime University, for providing real-world underwater images and videos. They also thank the anonymous reviews for their insightful comments and suggestions, and Editage (www.editage.cn) for English language editing.

DATA AVAILABILITY STATEMENT

The data that support the findings of this study are available from the corresponding author, upon reasonable request.

REFERENCES

[1] W. Yuan, C. Fu, R. Liu, and X. Fan, "SSoB: Searching a scene-oriented architecture for underwater object detection," *Vis. Comput.*, pp. 1–10, Sep. 2022.

[2] S. Pei and C. Chen, "Underwater images enhancement by revised underwater images formation model," *IEEE Access*, vol. 10, pp. 108817–108831, 2022, doi: 10.1109/ACCESS.2022.3213340.

[3] K. Gong and D. Hua, "Research on the method of color compensation and underwater image restoration based on polarization characteristics," in *Proc. 3rd Int. Conf. Comput. Vis., Image Deep Learn. Int. Conf. Comput. Eng. Appl. (CVIDL ICCEA)*, May 2022, pp. 746–751, doi: 10.1109/CVIDLICCEA56201.2022.9824370.

[4] N. M. A. Mohamed, L. Lin, W. Chen, and H. Wei, "Underwater image quality: Enhancement and evaluation," in *Proc. Cross Strait Radio Sci. Wireless Technol. Conf. (CSRSWTC)*, Dec. 2020, pp. 1–3, doi: 10.1109/CSRSWTC50769.2020.9372502.

[5] G. Hou, X. Zhao, Z. Pan, H. Yang, L. Tan, and J. Li, "Benchmarking underwater image enhancement and restoration, and beyond," *IEEE Access*, vol. 8, pp. 122078–122091, 2020, doi: 10.1109/ACCESS.2020.3006359.

[6] R. Lin, J. Liu, R. Liu, and X. Fan, "Global structure-guided learning framework for underwater image enhancement," *Vis. Comput.*, vol. 38, no. 12, pp. 4419–4434, Dec. 2022.

[7] C. Li, S. Tang, H. K. Kwan, J. Yan, and T. Zhou, "Color correction based on CFA and enhancement based on Retinex with dense pixels for underwater images," *IEEE Access*, vol. 8, pp. 155732–155741, 2020, doi: 10.1109/ACCESS.2020.3019354.

[8] Y. Liu, S. Rong, X. Cao, T. Li, and B. He, "Underwater image dehazing using the color space dimensionality reduction prior," in *Proc. IEEE Int. Conf. Image Process. (ICIP)*, Oct. 2020, pp. 1013–1017, doi: 10.1109/ICIP40778.2020.9190901.

[9] M. Wu, K. Luo, J. Dang, and D. Li, "Underwater image restoration using color correction and non-local prior," in *Proc. OCEANS*, Jun. 2017, pp. 1–5, doi: 10.1109/OCEANSE.2017.8084916.

[10] O. K. Athira and J. Babu, "Underwater image restoration using scene depth estimation technique," in *Proc. 3rd Int. Conf. Smart Syst. Inventive Technol. (ICSSIT)*, Aug. 2020, pp. 137–144.

[11] J. C. Guo, C. Y. Li, C. L. Guo, and S. J. Chen, "Research progress of underwater image enhancement and restoration methods," *J. Image Graph.*, vol. 22, no. 3, pp. 273–287, 2017.

[12] L. Li, H. G. Wang, and X. Liu, "Underwater image enhancement based on improved dark channel prior and color correction," *Acta Optica Sinica*, vol. 37, no. 12, 2018, Art. no. 1211003.

[13] N. C. Mhala and A. R. Pais, "A secure visual secret sharing (VSS) scheme with CNN-based image enhancement for underwater images," *Vis. Comput.*, vol. 37, no. 8, pp. 2097–2111, Aug. 2021.

[14] C. Li, C. Guo, W. Ren, R. Cong, J. Hou, S. Kwong, and D. Tao, "An underwater image enhancement benchmark dataset and beyond," *IEEE Trans. Image Process.*, vol. 29, pp. 4376–4389, 2020, doi: 10.1109/TIP.2019.2955241.

[15] A. J. R. Fairweather, M. A. Hodgetts, and A. R. Greig, "Robust scene interpretation of underwater image sequences," in *Proc. 6th Int. Conf. Image Process. Appl.*, Dublin, Ireland, 1997, pp. 660–664, doi: 10.1049/cp:19970977.

[16] M. Chambah, D. Semani, A. Renouf, P. Courtellemont, and A. Rizzi, "Underwater color constancy: Enhancement of automatic live fish recognition," *Proc. SPIE*, vol. 293, pp. 157–168, Dec. 2004.

[17] Y. Y. Schechner and N. Karpel, "Clear underwater vision," in *Proc. IEEE Comput. Soc. Conf. Comput. Vis. Pattern Recognit.*, vol. 1, Washington, DC, USA, Jul. 2004, doi: 10.1109/CVPR.2004.1315078.

[18] E. Trucco and A. T. Olmos-Antillon, "Self-tuning underwater image restoration," *IEEE J. Ocean. Eng.*, vol. 31, no. 2, pp. 511–519, Apr. 2006, doi: 10.1109/JOE.2004.836395.

[19] S. Bazeille, I. Quidu, L. Jaulin, and J. P. Malkasse, "Automatic underwater image pre-processing," in *Proc. Caracterisation Du Milieu Marin*, 2006, pp. 1–7.

[20] K. Iqbal, R. A. Salam, and A. Osman, "Underwater image enhancement using an integrated colour model," *IAENG Int. J. Comput. Sci.*, vol. 34, no. 2, pp. 239–244, 2007.

[21] D. Shi, Q. W. Li, X. N. Fan, and G. Y. Huo, "Underwater image enhancement algorithm based on Contourlet transform and multi-scale Retinex," *Laser Optoelectron. Prog.*, vol. 47, no. 4, 2010, Art. no. 041001.

[22] G. N. Lan, J. Li, and F. Ji, "Underwater image backscatter noise reduction based on wavelets," *Ocean Technol.*, vol. 29, no. 2, pp. 43–47, 2010.

[23] K. He, J. Sun, and X. Tang, "Single image haze removal using dark channel prior," *IEEE Trans. Pattern Anal. Mach. Intell.*, vol. 33, no. 12, pp. 2341–2353, Dec. 2011.

[24] J. Y. Chiang and Y. Chen, "Underwater image enhancement by wavelength compensation and dehazing," *IEEE Trans. Image Process.*, vol. 21, no. 4, pp. 1756–1769, Apr. 2012, doi: 10.1109/TIP.2011.2179666.

[25] C. Ancuti, C. O. Ancuti, T. Haber, and P. Bekaert, "Enhancing underwater images and videos by fusion," in *Proc. IEEE Conf. Comput. Vis. Pattern Recognit.*, Providence, RI, USA, Jun. 2012, pp. 81–88, doi: 10.1109/CVPR.2012.6247661.

[26] K. Singh, R. Kapoor, and S. K. Sinha, "Enhancement of low exposure images via recursive histogram equalization algorithms," *Optik*, vol. 126, no. 20, pp. 2619–2625, Oct. 2015.

[27] G. Singh, N. Jaggi, S. Vasamsetti, H. K. Sardana, S. Kumar, and N. Mittal, "Underwater image/video enhancement using wavelet based color correction (WBCC) method," in *Proc. IEEE Underwater Technol. (UT)*, Chennai, India, Feb. 2015, pp. 1–5, doi: 10.1109/UT.2015.7108303.

[28] C. Li and J. Guo, "Underwater image enhancement by dehazing and color correction," *J. Electron. Imag.*, vol. 24, no. 3, 2015, Art. no. 033023.

[29] A. Galdran, D. Pardo, A. Picon, and G. A. Alvarez, "Automatic red-channel underwater image restoration," *J. Vis. Commun. Image Represent.*, vol. 26, pp. 132–145, Jan. 2015.

[30] S. Zhang, T. Wang, J. Dong, and H. Yu, "Underwater image enhancement via extended multi-scale Retinex," *Neurocomputing*, vol. 245, pp. 1–9, Jul. 2017.

[31] S. Vasamsetti, N. Mittal, B. C. Neelapu, and H. K. Sardana, "Wavelet based perspective on variational enhancement technique for underwater imagery," *Ocean Eng.*, vol. 141, pp. 88–100, Sep. 2017.

[32] X. Sun, L. Liu, and J. Dong, "Underwater image enhancement with encoding-decoding deep CNN networks," in *Proc. IEEE Smart-World, Ubiquitous Intell. Comput., Adv. Trusted Comput., Scalable Comput. Commun., Cloud Big Data Comput., Internet People Smart City Innov. (SmartWorld/SCALCOM/UIC/ATC/CBDCom/IOP/SCI)*, San Francisco, CA, USA, 2017, pp. 1–6, doi: 10.1109/UIC-ATC.2017.8397462.

[33] T. Ueda, K. Yamada, and Y. Tanaka, "Underwater image synthesis from RGB-D images and its application to deep underwater image restoration," in *Proc. IEEE Int. Conf. Image Process. (ICIP)*, Taipei, Taiwan, Sep. 2019, pp. 2115–2119, doi: 10.1109/ICIP.2019.8803195.

[34] C. G. Dai, M. X. Lin, Z. Wang, D. Zhang, and Z. G. Guan, "Color compensation based on bright channel and fusion for underwater image enhancement," *Acta Optica Sinica*, vol. 38, no. 11, pp. 86–95, 2018.

[35] X. Wang, X. C. Zhu, C. Ning, and G. Lu, "Combination of dark-channel prior with sparse representation for underwater image restoration," *J. Electron. Inf. Technol.*, vol. 40, no. 2, pp. 264–271, 2018.

[36] T. P. Marques and A. B. Albu, "L^2UWE: A framework for the efficient enhancement of low-light underwater images using local contrast and multi-scale fusion," in *Proc. IEEE/CVF Conf. Comput. Vis. Pattern Recognit. Workshops (CVPRW)*, Jun. 2020, pp. 2286–2295.

[37] C. Li, S. Tang, and H. Wu, "Simple estimation of red channel's transmittance and balanced color correction for underwater image enhancement," in *Proc. 13th Int. Congr. Image Signal Process., Biomed. Eng. Informat. (CISP-BMEI)*, Oct. 2020, pp. 1132–1136, doi: 10.1109/CISP-BMEI51763.2020.9263505.

[38] Z. Guo, D. Guo, Y. Jiang, Q. Li, Z. Gu, H. Zheng, B. Zheng, and G. Wang, "Underwater image enhancement based on intrinsic images," in *Proc. OCEANS*, San Diego, CA, USA, Sep. 2021, pp. 1–5, doi: 10.23919/OCEANS44145.2021.9705714.

[39] J. Hu, Q. Jiang, R. Cong, W. Gao, and F. Shao, "Two-branch deep neural network for underwater image enhancement in HSV color space," *IEEE Signal Process. Lett.*, vol. 28, pp. 2152–2156, 2021, doi: 10.1109/LSP.2021.3099746.

[40] Y. Kang, Q. Jiang, C. Li, W. Ren, H. Liu, and P. Wang, "A perception-aware decomposition and fusion framework for underwater image enhancement," *IEEE Trans. Circuits Syst. Video Technol.*, vol. 33, no. 3, pp. 988–1002, Mar. 2023, doi: 10.1109/TCSVT.2022.3208100.

[41] A. AbuNaser, I. A. Doush, N. Mansour, and S. Alshattnawi, "Underwater image enhancement using particle swarm optimization," *J. Intell. Syst.*, vol. 24, no. 1, pp. 99–115, Mar. 2015.

[42] B. L. McGlamery, "A computer model for underwater camera systems," *Proc. SPIE*, vol. 208, pp. 221–231, Mar. 1980.

[43] I. Kansal and S. S. Kasana, "Improved color attenuation prior based image de-fogging technique," *Multimedia Tools Appl.*, vol. 79, nos. 17–18, pp. 12069–12091, May 2020.

[44] Y. Y. Schechner and N. Karpel, "Recovery of underwater visibility and structure by polarization analysis," *IEEE J. Ocean. Eng.*, vol. 30, no. 3, pp. 570–587, Jul. 2005, doi: 10.1109/JOE.2005.850871.

[45] I. Kansal and S. S. Kasana, "Fusion-based image de-fogging using dual tree complex wavelet transform," *Int. J. Wavelets, Multiresolution Inf. Process.*, vol. 16, no. 6, 2018, Art. no. 1850054, doi: 10.1142/s0219691318500546.

[46] S. Gao, K. Yang, C. Li, and Y. Li, "Color constancy using double-opponency," *IEEE Trans. Pattern Anal. Mach. Intell.*, vol. 37, no. 10, pp. 1973–1985, Oct. 2015.

[47] E. Reinhard, M. Adhikhmin, B. Gooch, and P. Shirley, "Color transfer between images," *IEEE Comput. Graph. Appl.*, vol. 21, no. 4, pp. 34–41, Jul./Aug. 2001.

[48] R. Liu, X. Fan, M. Zhu, M. Hou, and Z. Luo, "Real-world underwater enhancement: Challenges, benchmarks, and solutions under natural light," *IEEE Trans. Circuits Syst. Video Technol.*, vol. 30, no. 12, pp. 4861–4875, Dec. 2020, doi: 10.1109/TCSVT.2019.2963772.

[49] *URPC2019 Data Set*. Accessed: Nov. 11, 2020. [Online]. Available: https://github.com/mousecpn/DG-YOLO

[50] K. Panetta, C. Gao, and S. Agaian, "Human-visual-system-inspired underwater image quality measures," *IEEE J. Ocean. Eng.*, vol. 41, no. 3, pp. 541–551, Jul. 2016, doi: 10.1109/JOE.2015.2469915.

[51] Q. Jiang, Y. Gu, C. Li, R. Cong, and F. Shao, "Underwater image enhancement quality evaluation: Benchmark dataset and objective metric," *IEEE Trans. Circuits Syst. Video Technol.*, vol. 32, no. 9, pp. 5959–5974, Sep. 2022, doi: 10.1109/TCSVT.2022.3164918.

[52] M. Yang and A. Sowmya, "An underwater color image quality evaluation metric," *IEEE Trans. Image Process.*, vol. 24, no. 12, pp. 6062–6071, Dec. 2015, doi: 10.1109/TIP.2015.2491020.

JING QIAN (Member, IEEE) received the master's degree in automation from the Qingdao University of Technology, China, in 2018. He is currently pursuing the Ph.D. degree with the Institute of Intelligent Machines, Chinese Academy of Sciences. From 2019 to 2020, he had a learning exchange with the Peng Cheng Laboratory, Shenzhen, China. His current research interests include machine vision, underwater image processing, and image quality.

BIN KONG (Member, IEEE) received the B.Sc. degree in computer science from Fudan University, China, in 1986, and the Ph.D. degree in pattern recognition and intelligent systems from the University of Science and Technology of China (USTC), in 2005. She has been a Researcher with the Institute of Intelligent Machines, Chinese Academy of Sciences, since 1986, and a Ph.D. Supervisor with USTC, since 2009. Her current research interests include image processing and analysis, machine vision, and perception system for intelligent robots.

JING YANG (Member, IEEE) received the Ph.D. degree in computer science from the Hefei University of Technology, Hefei, China, in 2009. From 2009 to 2020, she was an Associate Researcher with the Institute of Intelligent Machines, Chinese Academy of Sciences. She is currently an Associate Professor with Hefei University. Her current research interests include machine vision, intelligent computing, and complex networks.